Inorganic Chemistry
Article

Inorg. Chem. **2010**, *49*, 6859–6864 **6859**
DOI: 10.1021/ic100214v

First-Principles Prediction on the High-Pressure Structures of Transition Metal Diborides (TMB_2, TM = Sc, Ti, Y, Zr)

Meiguang Zhang,[†,‡] Hui Wang,[†] Hongbo Wang,[†] Xinxin Zhang,[†] Toshiaki Iitaka,[§] and Yanming Ma*[,†]

[†]*National Laboratory of Superhard Materials, Jilin University, Changchun 130012, People's Republic of China,*
[‡]*Department of Physics, BaoJi University of Arts and Sciences, Baoji 712007, People's Republic of China, and*
[§]*Computational Astrophysics Laboratory, RIKEN, 2-1 Hirosawa, Wako, Saitama 351-0198, Japan*

Received February 3, 2010

We have extensively explored the high-pressure structures of transition-metal diborides (TMB_2, TM = Sc, Ti, Y, and Zr) stabilized with the AlB_2-type structure at ambient pressure by using first-principles structural prediction. We find two novel high-pressure structures: (i) a monoclinic structure (*C*2/*m*, Z = 4) for ScB_2 and YB_2 stable above 208 and 163 GPa, respectively; and (ii) a tetragonal α-$ThSi_2$-type phase ($I4_1/amd$, Z = 4) for TiB_2 stable above 215 GPa. Our calculations show that the electron transfer from transition-metals TM to B under pressure might be the main cause for the structural phase transitions. Further phonon and hardness calculations suggest that α-$ThSi_2$ phase of TiB_2 is quenchable to ambient pressure and possesses excellent mechanical property with a Vickers hardness of 29.8 GPa. Interestingly, ZrB_2 is quite stable and persists on the ambient-pressure AlB_2-type structure up to at least 300 GPa. We attribute the strong covalent hybridization between the transition-metal Zr and B to this ultrastability.

1. Introduction

Transition-metal diborides (TMB_2) have attracted much attention due to their unique physical and chemical properties in fundamental science and technological applications, such as high-melting point, hardness, high-thermal conductivity, chemical inertness etc.[1−6] TMB_2 typically crystallizes in the well-known AlB_2-type structure (*P*6/*mmm*, Z = 1) with TM and B atoms sitting at the origin and (1/3, 2/3, 1/2) sites, respectively (Figure 1a), in which the coplanar graphite-like B layers are present alternatively with the close-packed TM sheets. Recently, intensive interest for TMB_2 compounds has re-emerged after the discovery of high superconductivity in AlB_2-type MgB_2.[7]

High-pressure research is leading to the identification of novel behavior of solids and the exploration of potential technological materials, since pressure could significantly alter the electronic bonding state to modify the physical properties and/or then induce the structural phase transition. However, the high-pressure behaviors of AlB_2-type TMB_2 compounds are least studied, and there is lack of confirmed reports on the existence of pressure-induced phase transitions. Experimentally, the compressibility measurements by using X-ray diffraction techniques for TiB_2 up to 65 GPa,[8] ZrB_2 and VB_2 up to 50 GPa,[9] and HfB_2 up to 30 GPa[10] were performed, and some related mechanical characteristics were investigated, but no obvious phase transitions were observed in any of these compounds. Theoretically, Ma et al.[11] first reported a nonsuperconducting high-pressure orthorhombic KHg_2-type polymorph (*Imma*, Z = 4) of MgB_2 stable above 190 GPa through ab initio evolutionary simulations. The thermodynamic properties of TiB_2[12] and elastic and electronic properties of NbB_2[13] under pressure were calculated, and the results do not suggest structural transformations over a wide range of pressure (0−200 GPa).

As an exploratory research, we here present extensive structure searches to uncover the high-pressure structures of TMB_2 (TM = Sc, Ti, Y, and Zr) up to 300 GPa using the

*E-mail: mym@jlu.edu.cn.

(1) Post, B. *Refractory Binary Borides, Metallo-Boron Compounds and Boranes*; Wiley: New York, 1964.
(2) Matkovich, M. I. *Boron and Refractory Borides*; Springer: Berlin, Germany, 1977.
(3) Mitterer, C. *J. Solid State Chem.* **1997**, *133*, 279–291.
(4) Ivanovskaya, V. V.; Enyashin, A. N.; Ivanovskii, A. L. *Inorg. Mater.* **2004**, *40*, 134–143.
(5) Basu, B.; Raju, B. G.; Suri, A. K. *Int. Mater. Rev.* **2005**, *51*, 352–374.
(6) Mishra, S. K.; Rupa, P. K. P.; Pathak, L. C. *Thin Solid Films* **2007**, *17*, 6884–6889.
(7) Nagamatsu, J.; Nakagawa, N; Muranaka, T.; Zenitani, Y.; Akimitsu, J. *Nature* **2001**, *410*, 63–64.
(8) Amulele, G. M.; Manghnani, M. H.; Somayazulu, M. *J. Appl. Phys.* **2006**, *99*, 023522.
(9) Pereira, A. S.; Perottoni, C. A.; Jornada, J. A. H. d.; Leger, J. M.; Haines, J. *J. Phys.:Condens. Matter* **2002**, *14*, 10615–10618.
(10) Halevy, I.; Beck, A.; Yaar, I.; Kahane, S.; Levy, O.; Auster, E.; Ettedgui; Caspi, E. N.; Rivin, O.; Berant, Z.; Hu, J. *Hyperfine Interact.* **2007**, *177*, 57–64.
(11) Ma, Y. M.; Wang, Y. C.; Oganov, A. R. *Phys. Rev. B: Condens. Matter Mater. Phys.* **2009**, *79*, 054101.
(12) Peng, F.; Fu, H. Z.; Cheng, X. L. *Physica B* **2007**, *400*, 83–87.
(13) Li, X. F.; Ji, G. F.; Zhao, F.; Chen, X. R.; Alfe, D. *J. Phys.: Condens. Matter* **2009**, *21*, 025505.

Published on Web 06/25/2010

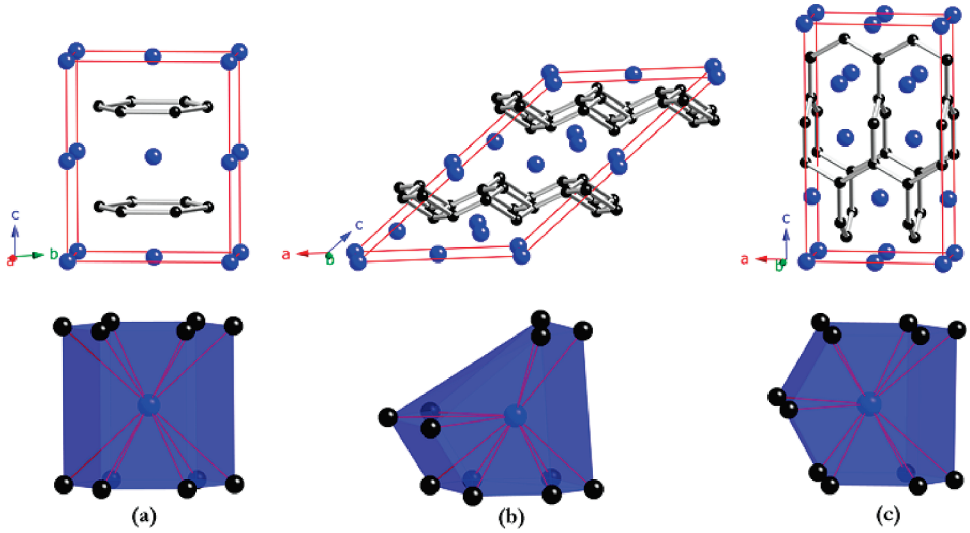

Figure 1. Crystal structures (above) and corresponding building blocks (down) of ambient pressure and the predicted high-pressure phases: AlB_2 (a), monoclinic $C2/m$ (b), and α-$ThSi_2$ (c) phases. The large and small spheres represent TM and B atoms, respectively. For $C2/m$ ScB_2 at 215 GPa, the lattice parameters are $a = 7.134$, $b = 2.664$, and $c = 5.791$ Å and $\beta = 139.2°$, with B1 at 4*i* (0.5496, 0, 0.9148), B2 at 4*i* (0.8838, 0, 0.1597), and Sc at 4*i* (0.7109, 0, 0.6441); for $C2/m$ YB_2 at 170 GPa, the lattice parameters are $a = 7.364$, $b = 2.812$, and $c = 6.007$ Å and $\beta = 134.9°$, with B1 at 4*i* (0.6230, 0, 0.3053), B2 at 4*i* (0.9374, 0, 0.5750) and Y at 4*i* (0.7799, 0, 0.8510); for α-$ThSi_2$ TiB_2 at 0 GPa, the lattice parameters are $a = 3.113$ and $c = 10.554$ Å, with B at 8*e* (0, 0, 0.0831) and Ti at 4*b* (0, 0, 0.5), respectively.

ab initio evolutionary algorithm.[14−21] Our target is to identify the possible high-pressure polymorphs of these borides and then to further explore their mechanical properties at a fundamental level. Our results show that ZrB_2 persists up to 300 GPa within an ambient-pressure AlB_2-type structure, while pressure-induced transitions into monoclinic phases ($C2/m$, $Z = 4$) for ScB_2 at 208 GPa and YB_2 at 163 GPa, and a tetragonal α-$ThSi_2$ structure ($I4_1/amd$, $Z = 4$) for TiB_2 at 215 GPa was first predicted. The phase transformation mechanism has been fully discussed.

2. Computational Method

The evolutionary variable-cell high-pressure structure predictions were performed at 80, 240, and 300 GPa with systems containing one to four formula units (f.u.) in the simulation cell by using the USPEX code,[14−16] designed to search for the structure possessing the lowest free energy at given P/T conditions. The most significant feature of this methodology is the capability of predicting the stable structure with only the knowledge of the chemical composition. In the evolutionary search process, the first generation of structures was always produced randomly. All produced structures were relaxed at constant pressures, and the enthalpy was used as a fitness function. Discarding the worst (i.e., highest enthalpy) structures, the new generation was produced from the best 60% of the structures in the previous generation. New structures were created by (i) heredity (combining spatially coherent slabs cut from two parent structures in a random direction at random positions and with random thickness) and (ii) lattice mutation. In addition, the best structure of a generation was carried over into the next generation. The underlying structure relaxations were performed using density functional theory within the generalized gradient approximation (GGA),[22] as implemented in the Vienna ab initio simulation package (VASP).[23] The electron−ion interaction was described by means of projector-augmented wave method,[24] which called for a d-electron as valence states for all transition metals. The electronic wave functions were expanded in a plane-wave basis set with a well converged cutoff energy of 420 eV for all cases. Monkhorst−Pack *k* point meshes[25] with a grid of 0.035 $Å^{-1}$ for Brillouin zone sampling were chosen to ensure the total energies converged to be better than ∼1 meV/f.u. Phonon frequencies were calculated using direct supercell, which uses the forces obtained by the Hellmann−Feynaman theorem.[26] Crystal orbital Hamiltonian population[27](COHP) was used for bond analysis, as implemented in the SIESTA package.[28,29] Single crystal elastic constants were determined from evaluation of stress tensor generated small strain and bulk modulus, shear modulus, Young's modulus and Poisson's ratio were thus estimated by using the Voigt−Reuss−Hill approximation.[30] The theoretical Vickers hardness was estimated by using the Šimůnek model.[31]

(14) Oganov, A. R.; Glass, C. W. *J. Chem. Phys.* **2006**, *124*, 244704.
(15) Oganov, A. R.; Glass, C. W.; Ono, S. *Earth Planet Sci. Lett.* **2006**, *241*, 95–103.
(16) Oganov, A. R.; Glass, C. W. *J. Phys.: Condens. Matter* **2008**, *20*, 064210.
(17) Gao, G. Y.; Oganov, A. R.; Bergara, A.; Martinez-Canales, M; Cui, T.; Iitaka, T.; Ma, Y. M.; Zou, G. T. *Phys. Rev. Lett.* **2008**, *101*, 107002.
(18) Li, Q.; Ma, Y. M.; Oganov, A. R.; Wang, H. B.; Wang, H.; Xu, Y.; Cui, T.; Mao, H. K.; Zou, G. T. *Phys. Rev. Lett.* **2009**, *102*, 175506.
(19) Ma, Y. M.; Oganov, A. R.; Li, Z. W.; Xie, Y.; Kotakoski, J. *Phys. Rev. Lett.* **2009**, *102*, 065501.
(20) Oganov, A. R.; Chen, J. H.; Gatti, C.; Ma, Y. Z.; Ma, Y. M.; Glass, C. W.; Liu, Z. X.; Yu, T.; Kurakevych, O. O.; Solozhenko, V. L. *Nature* **2009**, *453*, 863–867.
(21) Ma, Y. M.; Eremets, M.; Oganov, A. R.; Xie, Y.; Trojan, I.; Medvedev, S. A.; Lyakhov, O.; Valle, M.; Prakapenka, V. *Nature* **2009**, *458*, 182–185.
(22) Perdew, J. P.; Burke, K.; Ernzerhof, M. *Phys. Rev. Lett.* **1996**, *77*, 3865–3868.
(23) Kresse, G; Furthmüller, J. *Phys. Rev. B: Condens. Matter Mater. Phys.* **1996**, *54*, 11169–11186.
(24) Blöchl, P. E. *Phys. Rev. B: Condens. Matter Mater. Phys.* **1994**, *50*, 17953–17979.
(25) Monkhorst, H. J.; Pack, J. D. *Phys. Rev. B: Solid State* **1976**, *13*, 5188–5192.
(26) Parlinski, K.; Li, Z. Q.; Kawazoe, Y. *Phys. Rev. Lett.* **1997**, *78*, 4063–4066.
(27) Dronsowski, R.; Blöchl, P. E. *J. Phys. Chem.* **1993**, *97*, 8617–8624.
(28) Ordejn, P.; Soler, J. M. *Phys. Rev. B: Condens. Matter Mater. Phys.* **1996**, *53*, 10441–10444.
(29) Artacho, E.; Snchez-Portal, D.; Ordejn, P.; Garcia, A.; Soler, J. M. *Phys. Status Solidi B* **1999**, *215*, 809–817.
(30) Hill, R. *Proc. Phys. Soc. London* **1952**, *65*, 350.
(31) Šimůnek, A. *Phys. Rev. B: Condens. Matter Mater. Phys.* **2007**, *75*, 172108.

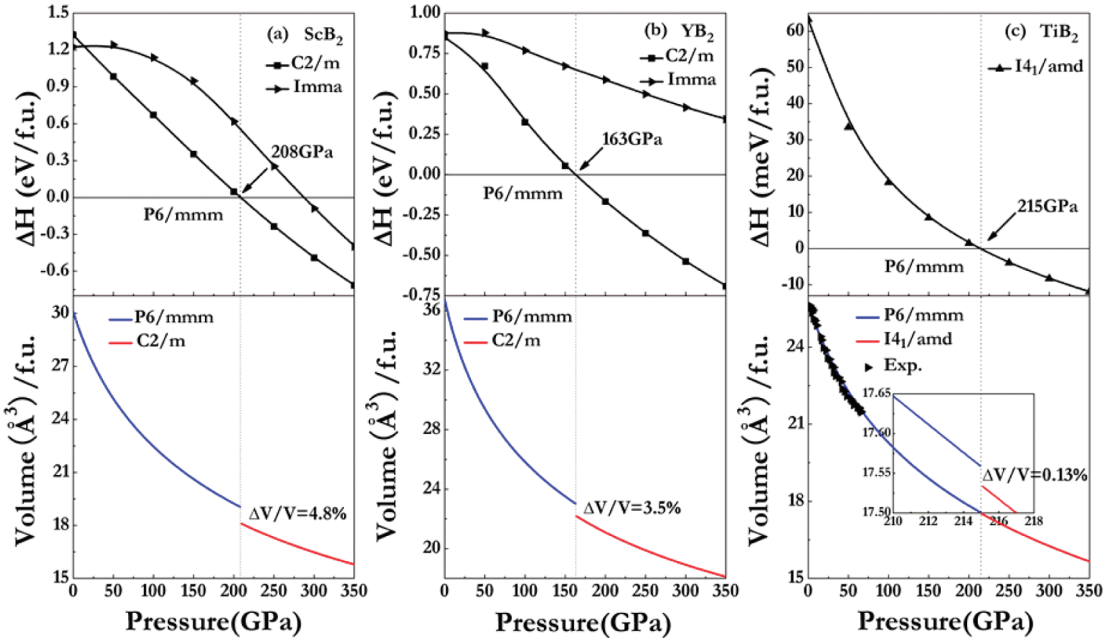

Figure 2. Enthalpy of the monoclinic $C2/m$ and α-$ThSi_2$ phases (relative to AlB_2) with pressure (above) and the $P-V$ curves (down) of ScB_2 (a), YB_2 (b), and TiB_2 (c).

3. Results and Discussion

For all TMB_2 compounds at 80 GPa, our simulations with the only input of chemical composition of TM:B = 1:2 predicted the most stable structure to be AlB_2 phase, in complete agreement with experiments. For higher pressure at 240 GPa and 300 GPa, a new stable monoclinic phase $C2/m$ having 4 f.u./cell (Figure 1b) was uncovered for both ScB_2 and YB_2, while a tetragonal α-$ThSi_2$-type phase with 4 f.u./cell (Figure 1c) was identified for TiB_2. More detailed structural information on the interatomic distances of these predicted phases are presented in Table 1. However, no high-pressure phase transitions were found for ZrB_2 up to 300 GPa. We have plotted out the enthalpy curves of the predicted structures relative to the ambient-pressure AlB_2-type structure in Figure 2, and the high-pressure KHg_2-type phase of MgB_2 unraveled earlier was also considered. It is confirmed from Figure 2 that the predicted $C2/m$ structure for ScB_2 and YB_2 becomes more stable than the AlB_2 phase above 208 and 163 GPa, respectively, while α-$ThSi_2$ structure for TiB_2 stabilizes above 215 GPa. Moreover, we have performed the calculations on the phonon dispersion curves of $C2/m$-ScB_2 and -YB_2 and α-$ThSi_2$-TiB_2 at 300 GPa. No imaginary phonon frequencies were found to confirm the structural stability of these new polymorphs.

The calculated equation of states by fitting the total energy vs volume data into the third-order Birch−Murnaghan equation[32] is shown in Figure 2. The results suggest that $AlB_2 \rightarrow C2/m$ phase transition is first-order with clear volume drops of 4.8 and 3.5% for ScB_2 and YB_2, respectively. The formation of a monoclinic $C2/m$ phase with a wrinkled boron layer resulted from the strong distortion of the planar B-sublattice of the AlB_2 phase and the concomitant displacement of TM atoms. The wrinkled B layer is composed of hexagonal and quadrangle B rings alternately. Intriguingly, the TM hendecahedron (Figure 1b), being centered by B atoms, is pointing alternately upward and downward along the crystallographic c axis. At the transition, the fourth B−B σ bonds (sp^3 hybridization, bond length is 1.608 and 1.662 Å for ScB_2 and YB_2, respectively) are constructed within the puckered layer in addition to the retaining of sp^2 bonding character (bond length is 1.580/1.591 for ScB_2 and 1.630/1.686 Å for YB_2), however, there is no formation of the new B−B bond between the adjacent wrinkled layers, as confirmed by the electron density calculation. Interestingly, $AlB_2 \rightarrow$ α-$ThSi_2$ phase transition in TiB_2 is also a first-order but with only a tiny volume drop 0.13% (inset to Figure 2c). The formation of the α-$ThSi_2$ structure is a result of dramatic B network change. The B hexagons are cut and connected with each other by twisting alternately 90° so as to form three-dimensional intersecting honeycomb stacks running along c axes (Figure 1c), and each B atom maintains the sp^2 bonding character. Ti atoms have 12 nearest B neighbors at the intersections, similar to those in AlB_2 and monoclinic $C2/m$ phases.

Table 1. Selected Interatomic Distances (Å) in $C2/m$-ScB_2 at 215 GPa, $C2/m$-YB_2 at 170 GPa, and α-$ThSi_2$-TiB_2 at 0 GPa

	distance			distance
	$C2/m$-ScB_2	$C2/m$-YB_2		α-$ThSi_2$-TiB_2
B1−B1	1.591	1.686	B−B	1.559
B1−B2	1.580	1.630		1.573
	1.608	1.662	Ti−B	2.074
B2−B2	1.870	1.989		2.082
TM−B1	2.084	2.276	Ti−Ti	3.063
	2.148	2.302		
	2.196	2.466		
	2.553	2.609		
TM−B2	2.164	2.275		
	2.165	2.279		
	2.205	2.339		
	2.276	2.578		
TM−TM	2.061	2.348		
	2.506	2.548		
	2.664	2.812		

The total and site projected density of states (DOS) of these diborides were plotted in Figure 3, and one can clearly see that all TMB_2 compounds are metals in their crystalline

(32) Birch, F. *J. Geophys. Res.* **1978**, *83*, 1257–1268.

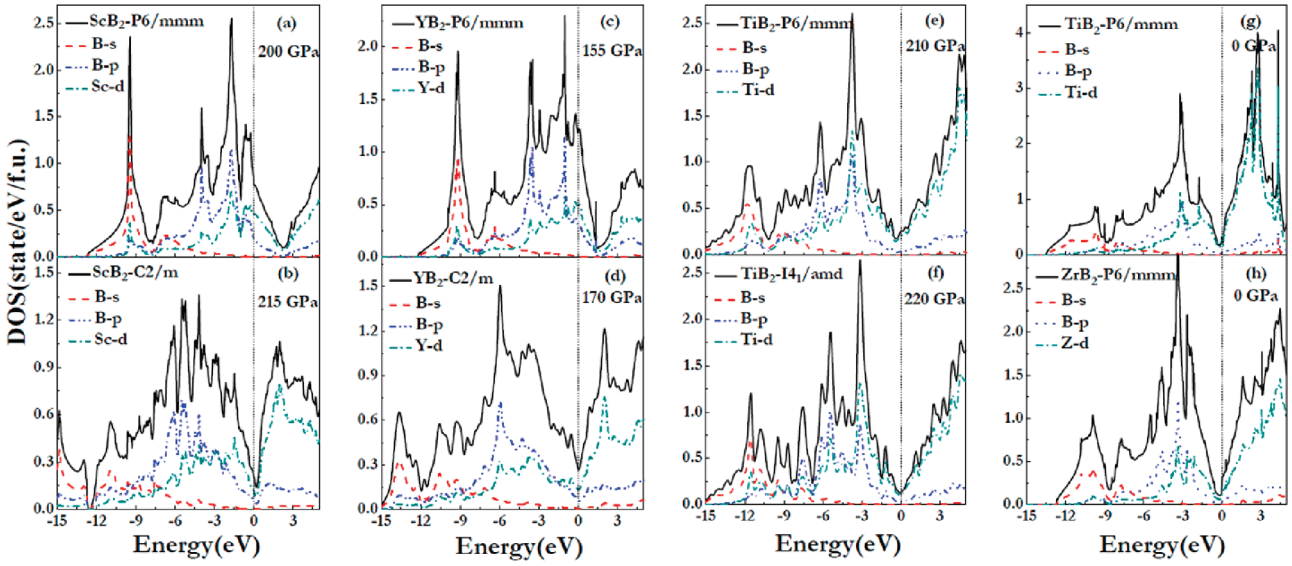

Figure 3. Total and partial DOS curves for AlB_2-type ScB_2 at 200 GPa (a), $C2/m$ phase of ScB_2 at 215 GPa (b), AlB_2-type YB_2 at 155 GPa (c), $C2/m$ phase of YB_2 at 170 GPa (d), AlB_2-type TiB_2 at 210 GPa (e), α-$ThSi_2$ phase of TiB_2 at 220 GPa (f), AlB_2-type TiB_2 at 0 Gpa (g), and AlB_2-type ZrB_2 at 0 Gpa (h). The vertical dashed lines denote the Fermi level.

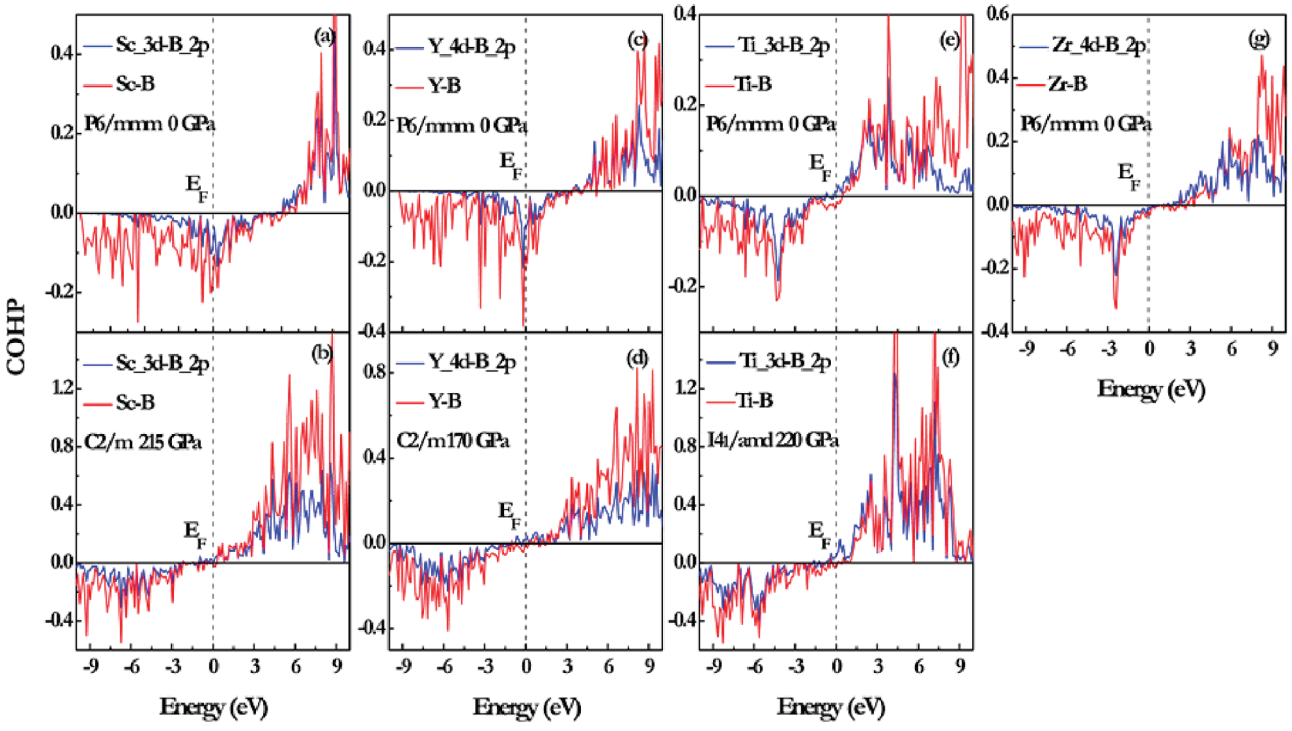

Figure 4. COHP curves for total TM-B interaction and partial TM-d−B-p interaction in AlB_2-type ScB_2 at 0 GPa (a), $C2/m$-ScB_2 at 215 GPa (b), AlB_2-type YB_2 at 0 GPa (c), $C2/m$-YB_2 at 170 GPa (d), AlB_2-type TiB_2 at 0 GPa (e), α-$ThSi_2$-TiB_2 at 220 GPa (f), and AlB_2-type ZrB_2 at 0 GPa (g). The vertical dashed lines denote the Fermi level.

states. The typical feature of the total DOS is the presence of a "pseudogap" (a sharp valley around the Fermi energy), the borderline between the bonding and antibonding states.[33−37] The calculated crystal overlap Hamilton population (COHP) shows that the bonding states of TiB_2 and ZrB_2 are completely filled (Figure 4e and g) with the Fermi energy located exactly at the "pseudogap". It is noteworthy that the bonding states are mainly attributed to the strong covalent interaction of TM-d and B-2p orbitals near the Fermi level (E_F). It is found that at the transition E_F shifts toward the lower energy and lies right at the pseudogap with a much lower electronic density of state [$N(E_F)$]. It is known that for the most stable structure there is enough room to accommodate all its

(33) Xu, J. H.; Freeman, A. J. *Phys. Rev. B: Condens. Matter Mater. Phys.* **1990**, *41*, 12553–12561.
(34) Burdett, J. K.; Canadell, E.; Miller, G. J. *J. Am. Chem. Soc.* **1986**, *108*, 6561–6568.
(35) Wang, X. B.; Tian, D. C.; Wang, L. L. *J. Phys.: Condens. Matter* **1994**, *6*, 10185–10192.
(36) Grechne, G. E.; Ushakova, N. V.; Kervalishvili, P. D.; Kvachantiradze, G. G.; Kharebov, K. S. *Low Temp. Phys.* **1997**, *23*, 217–219.
(37) Vajeeston, P.; Ravindran, P.; Ravi, C.; Asokamani, R. *Phys. Rev. B: Condens. Matter Mater. Phys.* **2001**, *63*, 045115.

Table 2. Calculated s, p, and d Electrons at Two Different Atomic Sites of AlB_2-type TMB_2 Compounds under Different Pressures[a]

	ScB_2					YB_2					TiB_2				
	$Sc(3p^63d^14s^2)$			$B(2s^22p^1)$		$Y(4p^64d^15s^2)$			$B(2s^22p^1)$		$Ti(3p^63d^24s^2)$			$B(2s^22p^1)$	
GPa	s	p	d	s	p	s	p	d	s	p	s	p	d	s	p
0	1.93	6.23	1.66	0.98	2.61	2.0	6.11	1.77	1.02	2.54	1.90	6.22	2.73	0.93	2.64
50	1.80	6.11	1.78	0.95	2.71	1.83	5.94	1.99	0.98	2.64	1.80	6.13	2.81	0.91	2.72
100	1.70	6.02	1.87	0.94	2.76	1.69	5.84	2.16	0.96	2.69	1.73	6.07	2.87	0.90	2.77
150	1.63	5.95	1.95	0.94	2.80	1.57	5.77	2.31	0.95	2.73	1.67	6.01	2.92	0.89	2.81
200	1.57	5.89	2.01	0.93	2.84						1.62	5.95	2.97	0.89	2.84

[a] (TM = Sc, Y, and Ti).

Table 3. Calculated Elastic Constants C_{ij}, Bulk Modulus B, Shear Modulus G, Young's Modulus E, and Hardness H_v in GPa[a]

		C_{11}	C_{12}	C_{13}	C_{33}	C_{44}	C_{66}	B	G	E	ν	H_v
$P6/mmm$-TiB_2												
	this work	652	76	115	461	259	288	262	256	579	0.132	33.6
	theory[b]	626	68	102	444	240	279	245				
	expt[c]	660	48	93	432	260	306	240	259	569		
	expt[d]											33.7
$I4_1/amd$-TiB_2												
	this work	569	125	91	668	273	271	269	262	593	0.132	29.8

[a] Also shown is Poisson's ratio ν and available experimental hardness (GPa). [b] Ref 12. [c] Ref 42. [d] Ref 43.

valence electrons into bonding states so as to bring the E_F to a valley position separating bonding and antibonding states (pseudogap) favorable for structural stability. Therefore, the formation of $C2/m$ and α-$ThSi_2$-type phases is energetically more favorable compared to the AlB_2 phase.

To explore the underlying mechanism for these phase transitions at a fundamental level, the charge transfer of AlB_2-type TMB_2 (TM = Sc, Y, and Ti) compounds with pressure were calculated and listed in Table 2. It is clearly seen that B-s electrons remain nearly invariant on the whole, but B-p and TM-d electrons increase continuously with the sacrifice of TM-s and -p electrons. This clearly indicates the charge transfer from TM-s and -p to TM-d and B-p orbitals under compression. According to the theory by Friedel[38] and Gellatt et al,[39] the essential contribution to the cohesion of the TMB compounds is the broadening of TM-d orbital and the hybridization between TM-d and B-p orbital, which can basically be regarded as the main cause for the variation of stability. Based on the rigid-band model, both ScB_2 and YB_2 within AlB_2 structures have nine valence electrons per unit cell, and their bonding states are not fully occupied. As a result, they have a larger $N(E_F)$ (Figure 3a and c) which is not most favorable for structural stability. Upon compression, their bonding states are gradually filled by the contributed electrons from TM-s and -p orbitals through charge transfer. This results in a gradual shift of E_F to a pseudogap and eventually in the stabilization of the monoclinic $C2/m$ structure with a nearly perfect localization of E_F at the pseudogap. Meanwhile, the COHP curves (Figure 4b and d) show that after the transitions into the monoclinic $C2/m$ phase all electrons in the occupied bands are in bonding states, while those states in vacant bands are antibonding states. Compared to ScB_2 and YB_2, TiB_2 possesses 10 valence electrons, and its bonding states are almost fully filled, and antibonding states are unoccupied with the presence of pseudogap at E_F at ambient pressure. Under pressure, its bonding states are already filled, and the antibonding states are getting occupied. Since the filling of antibonding states is less favorable for its structural stability, the compound is likely to adopt other energetically more favorable structures. Indeed, the pseudogap of TiB_2 lies right on the E_F in the α-$ThSi_2$ phase after the transition (Figures 3f and 4f). Therefore, charge transfer from TM-s and -p to TM-d and B-p under pressure should be the main cause for these structural phase transitions.

Among the elements of group four, Zr and Ti have the same valence configuration, however, ZrB_2 persists on the ambient-pressure AlB_2-type structure up to 300 GPa. To understand this exception, several aspects should be addressed. The outermost electrons in Zr are much more delocalized[37] and extend further from the nucleus compared to Ti. As a result, the valence electrons of Zr could have a stronger covalent hybridization with B atoms. It has been suggested in ref 37 that this increased hybridization effect might separate the bonding state from the antibonding states, leading to a lower $N(E_F)$. Indeed, it can be clearly seen that the $N(E_F)$ of ZrB_2 is lower (~0.101 states/eV/f.u.) than that of TiB_2, as shown in Figure 3g and h. Moreover, it is earlier proposed[33,40,41] that a lower $N(E_F)$ often characterizes a more stable structure. Therefore, it may require higher pressure to alter the electronic bonding states on the more stable ZrB_2 compared to TiB_2.

We here also checked the dynamical stabilities of the predicted $C2/m$ and α-$ThSi_2$ structures at ambient pressure by calculating the phonons. It is found that only α-$ThSi_2$-type TiB_2 has stable phonons among these predicted high-pressure structures. Therefore, only the mechanical properties of TiB_2 within AlB_2 and α-$ThSi_2$ structures were calculated and listed in Table 3. It is found that the whole set of elastic constants C_{ij} and other moduli (bulk modulus, Young's modulus and Poisson's ratio) of the AlB_2 phase are in excellent agreement

(38) Friedel, J. *The Physics of Metals*; Cambridge University Press: London, 1969.
(39) Gellatt, C. D. J.; Williams, A. R.; Moruzzi, V. L. *Phys. Rev. B: Condens. Matter Mater. Phys.* **1983**, *27*, 2005–2013.
(40) Xu, J. H.; Oguchi, T.; Freeman, A. J. *Phys. Rev. B: Condens. Matter Mater. Phys.* **1987**, *35*, 6940–6943.
(41) Xu, J. H.; Freeman, A. J. *Phys. Rev. B: Condens. Matter Mater. Phys.* **1989**, *40*, 11927–11930.

with the experiment results.[42] It is noted that α-$ThSi_2$ phase possesses a larger C_{33} (668 GPa for GGA) than that of the AlB_2 phase, indicating an enhanced incompressibility along the *c* direction. Moreover, the large shear modulus 262 GPa suggests that α-$ThSi_2$ phase can withstand shear strain to a large extent and is expected to be a hard material. The estimated theoretical Vickers hardness (H_v) for the AlB_2 and α-$ThSi_2$ phases in comparison with experimental data[43] were also summarized in Table 3. The predicted H_v of α-$ThSi_2$ phase is about 29.8 GPa, which is comparable to the known hard materials of α-SiO_2 (30.6 GPa).[44] The experimental synthesis of α-$ThSi_2$ phase of TiB_2 is thus demanded to make use of its mechanical properties.

4. Conclusion

In conclusion, we have reported two intriguing high-pressure phases for AlB_2-type TMB_2 (TM = Sc, Ti, Y, and Zr) under high pressure up to 300 GPa by using an evolutionary algorithm in crystal structural prediction. A monoclinic *C*2/*m* phase of ScB_2 and YB_2 has been predicted to be stable above 208 and 163 GPa, respectively, and a tetragonal α-$ThSi_2$-type structure of TiB_2 was uncovered at 215 GPa. The phase transitions from AlB_2 to monoclinic *C*2/*m* and α-$ThSi_2$-type phases are all first-order and can be attributed to the electron transfer from TM-s and -p to TM-d and B-p under pressure. As an exception, ZrB_2 holds on the ambient-pressure AlB_2-type structure up to at least 300 GPa, which may be due to the stronger covalent hybridization between Zr and B atoms when compared to other TMB_2 compounds. Among the predicted structures, only the α-$ThSi_2$-phase of TiB_2 can be stable at ambient pressure with the calculated Vickers hardness of 29.8 GPa and is important for technical applications.

Acknowledgment. We are thankful for financial support from the National Natural Science Foundation of China (NSFC) under grant no. 10874054, the NSFC awarded Research Fellowship for International Young Scientists under grant no. 10910263, the China 973 Program under Grant no. 2005CB724400, the research fund for Excellent young scientist in Jilin University (no. 200905003), and the 2007 Cheung Kong Scholars Program of China. M.Z. thanks the Baoji University of Arts and Sciences Key Research Grant no. ZK08112. The authors thank the computing facilities at RSCC system in RIKEN (Japan).

(42) Spoor, P. S.; Maynard, J. D.; Pan, M. J.; Hellmann, J. R.; Tanaka, T. *Appl. Phys. Lett*. **1997**, *70*, 1959–1961.
(43) Martienssen, W.; Warlimont, H. *Handbook of Condensed Matter and Materials Data*; Springer: Berlin, Germany, 2005.
(44) Gao, F. M.; He, J. L.; Wu, E. D.; Liu, S. M.; Yu, D. L.; Li, D. C.; Zhang, S. Y.; Tian, Y. J. *Phys. Rev. Lett*. **2003**, *91*, 015502.